A Spectroscopic Study of the Temperature Induced Modifications on Ferredoxin Folding and Iron−Sulfur Moieties†

Smilja Todorovic,‡,§ Sónia S. Leal,‡,§ Carlos A. Salgueiro,|| Ingo Zebger,⊥ Peter Hildebrandt,‡,⊥ Daniel H. Murgida,*,‡,# and Cláudio M. Gomes*,‡

Instituto de Tecnologia Química e Biológica, Universidade Nova de Lisboa, Av República EAN, 2781-901 Oeiras, Portugal, Departamento de Química, Faculdade de Ciências e Tecnologia, Universidade Nova de Lisboa, Quinta da Torre, 2825-114 Caparica, Portugal, Instituto de Tecnologia Química e Biológica, Universidade Nova de Lisboa, Oeiras, Portugal, Max-Volmer-Laboratorium für Biophysikalische Chemie, Institut für Chemie, Technische Universität Berlin, Sekr. PC14, Strasse des 17 Juni 135, D-10623 Berlin, Germany, and INQUIMAE-CONICET, Facultad de Ciencias Exactas y Naturales, Universidad de Buenos Aires, Ciudad Universitaria, Pab.2, piso 1, C1428EHA-Buenos Aires, Argentina

Received May 20, 2007; Revised Manuscript Received June 20, 2007

ABSTRACT: Thermal perturbation of the dicluster ferredoxin from *Acidianus ambivalens* was investigated employing a toolbox of spectroscopic methods. FTIR and visible CD were used for assessing changes of the secondary structure and coarse alterations of the [3Fe4S] and [4Fe4S] cluster moieties, respectively. Fine details of the disassembly of the metal centers were revealed by paramagnetic NMR and resonance Raman spectroscopy. Overall, thermally induced unfolding of *Aa*Fd is initiated with the loss of α-helical content at relatively low temperatures ($T_m^{app} \sim 44$ °C), followed by the disruption of both iron−sulfur clusters ($T_m^{app} \sim 53-60$ °C). The degradation of the metal centers triggers major structural changes on the protein matrix, including the loss of tertiary contacts ($T_m^{app} \sim 58$ °C) and a change, rather than a significant net loss, of secondary structure ($T_m^{app} \sim 60$ °C). This latter process triggers a secondary structure reorganization that is consistent with the formation of a molten globule state. The combined spectroscopic approach here reported illustrates how changes in the metalloprotein organization are intertwined with disassembly of the iron−sulfur centers, denoting the conformational interplay of the protein backbone with cofactors.

The folding and stability of proteins relies on a series of weak interactions of variable magnitudes, whose additive effect results in a stabilized three-dimensional fold. In the case of proteins that contain cofactors, especially metal centers, the impact and role of these cross-linkers in the protein overall folding, dynamics, and interconversion between native and non-native states turns out to be particularly relevant. A ferredoxin from the thermophile *Acidianus ambivalens* (*Aa*Fd) was shown to be an exceptionally good model for folding studies (*1*−*3*). This protein, which contains one $[3Fe4S]^{1+/0}$ and one $[4Fe4S]^{2+/1+}$ center in a canonical $(\beta\alpha\beta)_2$ fold (*4*), belongs to the Archaeal family of dicluster ferredoxins (*5*). Typically, these ferredoxins harbor a structural Zn^{2+} site with His/Asp coordination that stabilizes the N-terminal domain extension (*6*), which is also the case in *Aa*Fd[1] (*5*). In some isoforms within the family, this center is replaced by hydrophobic contacts, which results in a comparable stabilization of the domain (*7*). *Aa*Fd has a remarkable thermal and pH stability: at neutral pH it remains folded in the presence of 5 M GdmCl and it has a $T_m \sim 120$ °C (*1*). However, upon acidification down to pH 2.5 the protein folding and its iron−sulfur centers remain intact, although destabilized, making them amenable to thermal unfolding studies with T_m transitions well below the boiling point of water (*8*). Recently it was shown that a molten globule (Fd^{MG}) state is formed by thermally denaturing the native protein (Fd^N), followed by its (Fd^D) subsequent cooling at low pH (*8*):

$$Fd^N \xrightarrow{\text{heating}} Fd^D \xleftrightarrow{\text{cooling}} Fd^{MG}$$

In this work we address the thermal perturbation of *Aa*Fd at acidic pH using a set of complementary spectroscopic tools that provides a detailed description of the processes underly-

† The work was supported by Grants POCTI/BIO/43105 (to D.H.M.) and POCTI/QUI/37521 and POCTI/QUI/45758 (to C.M.G.) from the Fundação Ciência e Tecnologia (FCT/MCES, Portugal). S.S.L. is a recipient of a Ph.D. fellowship (SFRH/BD/18653/2004) from Fundação para a Ciência e Tecnologia (FCT/MCES, Portugal).

* C.M.G.: gomes@itqb.unl.pt; tel, +351214469332; fax, +351214411277. D.H.M.: dh.murgida@tu-berlin.de; tel, +541145763378 ext. 124; fax, +541145763341.

‡ Instituto de Tecnologia Química e Biológica, Universidade Nova de Lisboa.

§ These authors have equally contributed to the work.

|| Departamento de Química, Faculdade de Ciências e Tecnologia, Universidade Nova de Lisboa. Previous address: Instituto de Tecnologia Química e Biológica, Universidade Nova de Lisboa, Oeiras, Portugal.

⊥ Technische Universität Berlin.

Universidad de Buenos Aires.

[1] Abbreviations: ANS, 1-anilinonaphthalene-8-sulfonic acid; *Aa*Fd, *Acidianus ambivalens* ferredoxin; CD, circular dichroism; DLS, dynamic light scattering; Fe−S, iron−sulfur bond; FTIR, Fourier transform infrared; MG, molten globule; NMR, nuclear magnetic resonance; RR, resonance Raman; TXRF, total reflection X-ray fluorescence.

10.1021/bi700967g CCC: $37.00 © 2007 American Chemical Society
Published on Web 08/16/2007

ing the unfolding process at different levels of the metalloprotein organization.

MATERIALS AND METHODS

Protein. The dicluster ferredoxin was purified from *Acidianus ambivalens* grown at pH 2.5 and 80 °C (*9*). A cytosolic fraction of the cells (a kind gift from Prof. M. Teixeira, ITQB/UNL) was processed and the protein purified in two consecutive chromatographic steps as previously described (*5*). Protein purity was evaluated from the Abs_{410}/Abs_{280} ratio (~0.6) and SDS−PAGE. The integrity of both iron−sulfur clusters was evaluated by TXRF metal analysis (Prof. B. O. Kolbesen, Johann Wolfgang Goethe-Universität, Frankfurt), which yielded 6 ± 0.5 Fe per mol of ferredoxin. Protein stocks were kept as concentrated aliquots at −20 °C (40 mM potassium phosphate, 150 mM NaCl, pH 6.5).

Thermal Perturbation. Prior to the spectroscopic studies the purification buffer was freshly exchanged for 200 mM glycine buffer, pH 2.5. For NMR experiments the protein was lyophilized and then resuspended twice in 200 mM glycine/D_2O (99.96% atom) buffer solution, at pD 2.5. Thermal perturbation was performed by successively incubating *Aa*Fd (pH 2.5) at increasing temperatures, typically in the 20−90 °C range, during 5 min, with ca. 5−10 °C interval. After each incubation step the protein was cooled down to the measurement temperature.

Dynamic Light Scattering. Measurements were carried out in a Malvern Zetasizer nano ZS instrument, equipped with a 4 MW He−Ne Laser (632 nm). The protein (0.2 mM *Aa*Fd in 200 mM glycine buffer, pH 2.5) was filtered though a 0.22 μm filter prior to measurements, and a 1 × 1 cm quartz cuvette (Hellma) was used for measurements, at different incubation stages between 25 and 90 °C. The operating procedure was set to 20 runs, each being averaged for 20s. Data was analyzed by the DTS sotware (Malvern) in respect to the distribution of sizes by volume.

FTIR Spectroscopy. FTIR spectra were recorded on a Bruker Tensor 27 spectrometer equipped with a N_2(l)-cooled MCT detector at a spectral resolution of 4 cm^{-1}. About 10 μL of thermally treated sample (0.4 mM in 200 mM glycine buffer, pH 2.5) was injected into a gastight cell for liquids (path length 12 μm; CaF_2 windows). All measurement were done at 10 °C purging the sample compartment with dry air.

ANS Binding. Temperature incubated ferredoxin samples (typically 5 μM) were incubated with 250 μM 1-anilinonaphthalene-8-sulfonic acid (ANS) during 15−60 min prior to measurements. ANS fluorescence emission enhancement of bound ANS at 480 nm was evaluated upon excitation at 370 nm, and corrected for the background emission of a protein-free ANS solution in buffer (*10*).

CD Spectroscopy. CD spectra were recorded in a Jasco J-815 spectropolarimeter equipped with Peltier temperature control and cell stirring. Far UV−CD spectra were recorded using 1 mm path length polarimetrically certified cells (Hellma). Near-UV and visible CD measurements were carried out using rectangular 10 mm path length cells. Unless otherwise noted, experiments were carried out at 20 °C.

Resonance Raman. About 2 μL of 1.2 mM oxidized *Aa*Fd (200 mM glycine buffer, pH 2.5) was introduced into a N_2-(l)-cooled cryostat (Linkam) mounted on a microscope stage and cooled down to −190 °C. Spectra from the frozen sample were collected in backscattering geometry by using a confocal Raman microscope (Jobin Yvon, XY). The different excitation lines (413, 458, and 514 nm) were obtained either from a krypton ion laser (Coherent Innova 302) or from an argon ion laser (Coherent Innova 70). Typically, spectra were accumulated for 60 s with a laser power at sample of 9 mW. After polynomial background subtraction, spectra were treated with a home made component analysis software. For quantification of the thermally induced perturbation the positions and widths of the four bands assigned to the iron−sulfur clusters (*11*−*16*) were maintained constant and only their intensities were adjusted for each incubation temperature. The band fitting parameters for [3Fe4S], defined from spectra obtained with 514 nm excitation, allowed unambiguous determination of the [4Fe4S] band parameters in spectra obtained with the 413 nm laser.

^{1}H NMR. Spectra were collected at 500 MHz in a Bruker DRX500 spectrometer using a 5 mm inverse probe head with *z* gradients and a Eurotherm 818 temperature-control unit. The 1D ^{1}H NMR spectra of the oxidized *Aa*Fd were recorded at 23 °C with 32 k data points and water presaturation. Spectral width of 38 kHz, pulse width of 16 μs, and 1.2 s^{-1} pulse repetition rate were used. A total of 1024 transients were acquired. Free induction decays were subject to a 40 Hz exponential line broadening factor before Fourier transform. Chemical shifts are reported in parts per million (ppm), relative to tetramethylsilane, and the proton spectra were calibrated using the water signal as an internal reference (*17*). Control spectra recorded before and after lyophilization were identical (data not shown), indicating that the protein structure was not affected by the removal of water.

RESULTS AND DISCUSSION

Thermally induced structural perturbations of *Aa*Fd were investigated under acidic conditions by a variety of complementary spectroscopic methods which selectively monitor changes at different levels of the protein organization. A common perturbation protocol was adopted for the various spectroscopic studies. It consists of successive incubations of *Aa*Fd at increasing temperatures followed by cooling down to a reference temperature, prior to a spectroscopic measurement (see Materials and Methods). The apparent midpoint transitions (T_m^{app}) were determined by different spectroscopic techniques. The obtained T_m^{app} is the temperature at which the intensity of a given spectral feature characteristic of Fd^N falls to 50% of its initial value or, alternatively, the temperature at which a characteristic feature of the Fd^{MG} form has increased up to 50% of its maximum value.

FTIR was used to probe perturbations at the level of the secondary structure. The spectra show distinct changes as a function of the incubation temperature in the amide I region which are better visualized in a second derivative representation (Figure 1A). Specifically, we note large amplitude changes at 1630 cm^{-1} and smaller ones at 1690 cm^{-1} and 1649 cm^{-1}. The rise of the first two negative bands is ascribed to a formation of extended β-structures and turns, respectively (*18*−*21*), and renders T_m^{app} = 60 °C in both cases. Note that the appearance of a signal at 1630 cm^{-1} could also be indicative of the formation of intermolecular β-sheet aggregates. However, this possibility was ruled out

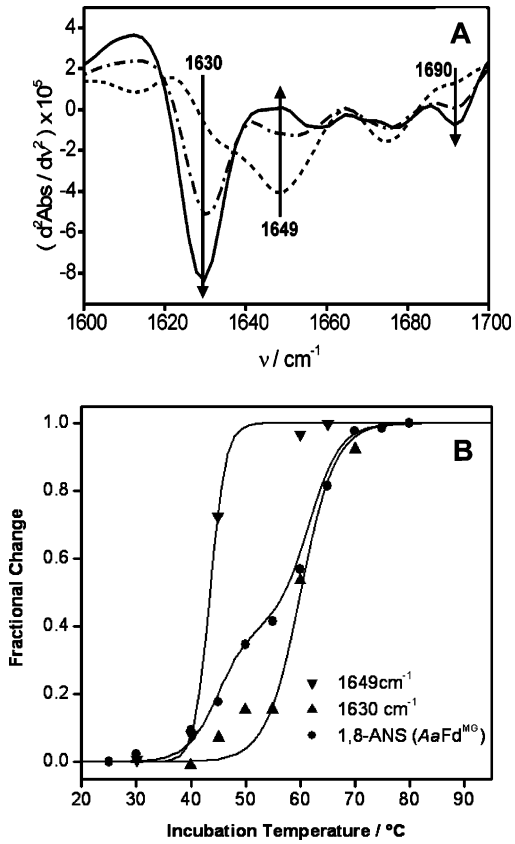

FIGURE 1: FTIR spectra (A) of *Aa*Fd recorded after thermal incubation at 30 °C (dash lines), 60 °C (dash−dot), and 70 °C (solid line), and temperature dependence profile (B) of the FTIR bands (up-triangles, 1630 cm^{-1}; down-triangles, 1649 cm^{-1}) and normalized 1,8-ANS fluorescence enhancement at 480 nm (circles). The solid lines represent sigmoidal fits (results are summarized in Table 1).

by the results of dynamic light scattering (DLS) experiments, which showed that no large size particles are formed during *Aa*Fd thermal perturbation. Rather, a ∼25% increase in the *Aa*Fd diameter is observed (from 6.9 ± 0.4 Å to 9.2 ± 0.2 Å) which is within the size range typically observed in molten globule states, which have a compactness identical to the native state, but exhibit a ∼10−30% increase in size (*22*). The growth of the positive band at 1649 cm^{-1} indicates a loss of α-helical content (*18*−*21*), which occurs with T_m^{app} = 44 °C. This value is distinctly lower than all other transition temperatures determined by the various methods (Table 1). Such a discrepancy cannot be attributed to the experimental error, although it is somewhat larger for the quantification of the 1649 cm^{-1} amplitude due to uncertainties in the background subtraction. Thus, regardless of the exact numerical value, it can be safely concluded that disorganization of the α-helices occurs at relatively low temperatures. Interestingly, no simultaneous changes are observed in the 1940−1945 cm^{-1} region, which would be indicative for the formation of an unordered (random coil) structure (*18*−*21*). Instead, β-structures are present, and this fact agrees with previous work showing that cooled thermally unfolded *Aa*Fd in acidic conditions leads to a molten globule state, which retains partial secondary structure (*8*). Changes in the secondary structure were also monitored by far-UV CD. Monitoring the signal at 222 nm, which comprises contributions both from β and α structures, yielded a transition at T_m^{app} = 60 °C (Table 1). The very low α-helical content of the protein (∼10%) impairs a resolution of the two types of secondary structure by far-UV CD, which was nevertheless achieved by FTIR.

Table 1: Apparent Midpoint Transition Temperatures Obtained by the Different Spectroscopic Methods

method	assignment	T_m^{app}/°C
FTIR	extended β-structures (1630 cm^{-1})	60 ± 2
	β-turns (1690 cm^{-1})	60 ± 2
	α-helices (1649 cm^{-1})	44 ± 5
ANS	molten globule formation (λ_{em} = 480 nm)	45 ± 2/60 ± 2
CD	Fe−S clusters	
	365 nm	58 ± 2
	422 nm	60 ± 2
	470 nm	64 ± 2
	575 nm	62 ± 2
	tertiary structure (285 nm)	58 ± 2
	secondary structure (222 nm)	62 ± 2
RR	[3Fe4S^B] (346 cm^{-1})	57 ± 2
	[3Fe4S^T] (366 cm^{-1})	53 ± 2
	[4Fe4S^B] (336 cm^{-1})	53 ± 2
	[4Fe4S^T] (358 cm^{-1})	53 ± 2
NMR	[3Fe4S] βH-Cys^{93}	57 ± 2
	[3Fe4S] βH-Cys$^{45/93}$	56 ± 2
	[3Fe4S] βH-Cys^{51}	56 ± 2
	[4Fe4S] βH-Cys^{86}	55 ± 2
	[4Fe4S] βH-Cys^{55}	55 ± 2
	[4Fe4S] βH-Cys^{89}	60 ± 2

The fraction of formed molten globule can be estimated from the increase of emission of 1,8-ANS at 480 nm. This fluorescent probe exhibits an increased emission upon binding to hydrophobic patches exposed in the MG state (*10*). A plot of the normalized 1,8-ANS emission enhancement as a function of incubation temperature denotes two transitions, T_m^{app} at 45 °C and 60 °C (Figure 1B), which correlate with the FTIR transitions. Therefore, the onset of molten globule formation is associated with this initial disruption of the α-helices. From this incubation temperature onward, *Aa*Fd undergoes further folding reorganization as the MG becomes significantly more populated in subsequent incubations, concomitantly with disruption of the Fe−S moieties (below). Additionally, loss of tertiary contacts as evidenced by monitoring the near-UV CD band at 285 nm occurs within the same temperature range (T_m^{app} = 58 °C; data not shown).

A first approach to evaluate coarse alterations of the Fe−S centers was based on visible CD spectroscopy. This technique provides better resolved features, eventually more informative than the visible absorption signature, which in *Aa*Fd comprises a main weak band at ca. 410 nm (*9*). The visible CD spectrum of *Aa*Fd displays a complex pattern (Figure 2A), including four bands that are attributable to both iron−sulfur cluster domains (*23*, *24*). The temperature-dependencies of the individual bands (Figure 2B) allow determination of different T_m^{app} values, as summarized in Table 1. These results indicate locally different thermal stability of the protein environment at the different metal centers. A detailed assignment, however, is precluded by the fact that none of the bands can be regarded as marker for an individual metal center.

As a more specific probe, RR spectroscopy was employed to monitor the disassembly of the individual clusters. In order

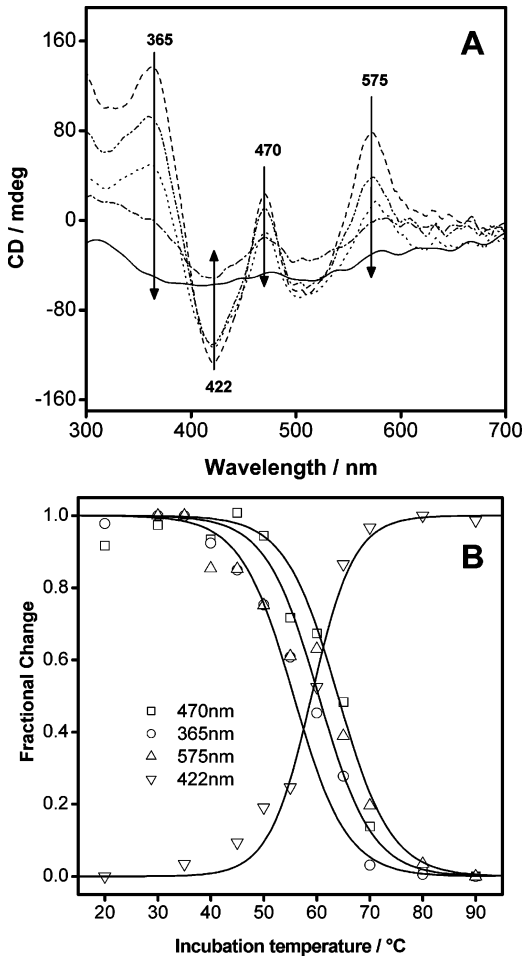

FIGURE 2: Visible CD spectra (A) of *Aa*Fd after thermal incubation at 30 °C (dash), 50 °C (dot−dot), 55 °C (dot), 65 °C (dash−dot), and 70 °C (solid), and temperature dependence profile (B) of visible CD bands at different wavelengths (squares, 470 nm; circles, 365 nm; triangles, 575 nm; and inverted triangles, 422 nm). The lines represent sigmoidal fits (results are summarized in Table 1).

to separate the spectral contributions from the [3Fe4S] and [4Fe4S] centers of *Aa*Fd, three different laser excitation lines (413, 458, and 514 nm) were used to achieve a differential enhancement of the RR bands associated with the two clusters. For all three excitation wavelengths, the most prominent RR band is observed at 346 cm^{-1} and is assigned to the stretching of the Fe−S−Fe bridges of the [3Fe-4S] center, [3Fe-4S^B] (*12*−*14*, *16*, *25*). This band is accompanied only by a weaker band at 366 cm^{-1}, upon excitation at 514 nm (data not shown), which is thus assigned to the terminal Fe−S vibrations of the same cluster, [3Fe4S^T] (*11*−*16*). The RR spectra recorded with 413 nm and 458 nm excitation show two additional features at 336 cm^{-1} and 358 cm^{-1} that are assigned to the Fe−S vibrations involving the bridging and terminal ligands of the [4Fe4S] cluster, respectively (*12*−*14*, *16*, *25*) ([4Fe4S^B] and [4Fe4S^T]), Scheme 1. As shown in Figure 3A, the RR bands of the [3Fe4S] center dominate the RR spectrum at 413 nm excitation (*12*). Nevertheless, the spectral contributions of the [4Fe4S] center can also be accurately determined by applying standard band fitting procedures. Besides the modes attributed to the bridging and terminal modes of [3Fe4S] and [4Fe4S] clusters, the RR spectrum also contains resolved bands at 386 cm^{-1} and 397 cm^{-1}. However, since these bands do not represent pure

Scheme 1: Cartoon Representing the General Ligation Scheme for the Dicluster *Aa*Fd

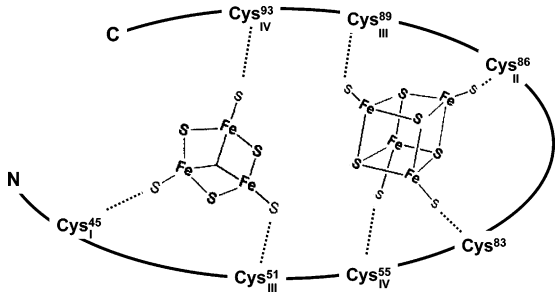

vibrational modes (*12*, *15*, *16*), they were not considered in the further analysis. This excitation line was thus used to monitor the temperature-dependent RR spectral changes and thermal disassembly of the two clusters. Figure 3B shows the intensity changes of the individual RR bands upon successive incubations of *Aa*Fd at increasing temperatures. An apparent transition at 53 °C is observed for all vibrational modes, except for [3Fe4S^B], for which a T_m^{app} = 57 °C is determined (Table 1). Although the difference of 4 °C is

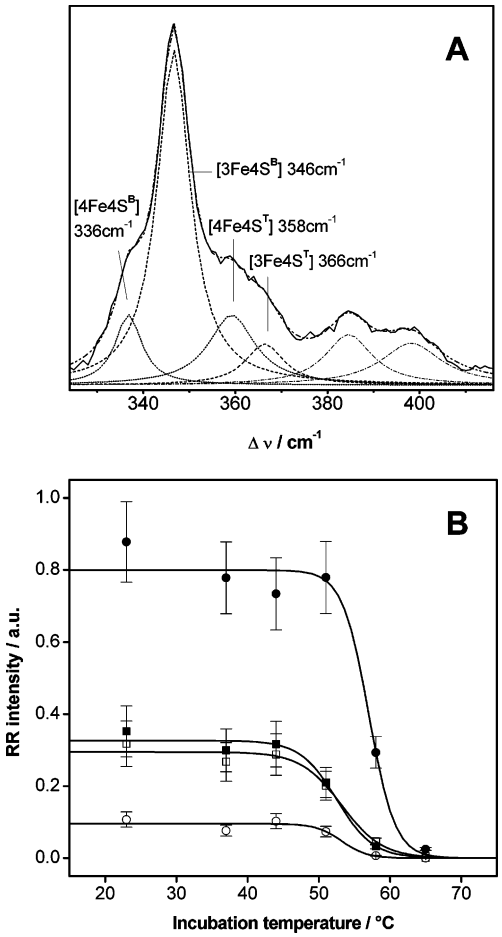

FIGURE 3: Experimental and band fitted RR spectra of (A) oxidized AaFd, and (B) relative intensities of [4Fe4S] (squares) and [3Fe4S] (circles) vibrational modes as a function of the incubation temperature. Experimental RR spectrum (solid line, A) was obtained from 1.2 mM AaFd (pH 2.5, no incubation), with 413 nm excitation and laser power of 9 mW at −190 °C. Overall fitted spectrum: dash-dot-dotted line. Component spectra: dashed line, [3Fe4S^B], 346 cm^{-1}, and [3Fe4S^T], 366 cm^{-1}; dotted line, [4Fe4S^B], 336 cm^{-1}, and [4Fe4S^{TI}, 358 cm^{-1}. The solid lines (B) represent sigmoidal fits (results are summarized in Table 1).

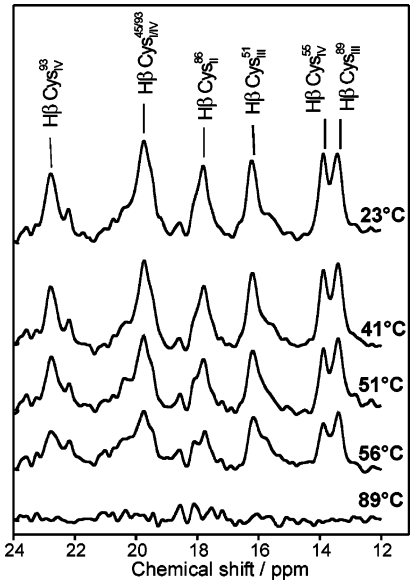

FIGURE 4: Low field region of a 1D ^{1}H NMR proton spectrum of *Aa*Fd. The assignments and incubation temperatures are indicated in the figure.

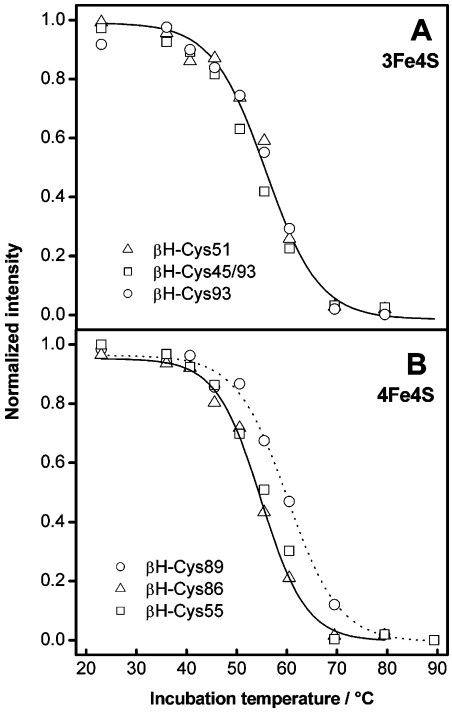

FIGURE 5: Thermal transitions of the cysteine ligands monitored from individual resonances for the [3Fe4S] clusters ligands (A) and [4Fe4S] cluster ligands (B). The lines represent sigmoidal fits (see Table 1).

relatively small and close to the experimental error, it is reproducibly observed.

Complementary structural information concerning the interaction of the iron−sulfur clusters and the protein chain was obtained by ^{1}H NMR. Inspection of the 1D ^{1}H NMR spectral window covering the downfield paramagnetic region of the *Aa*Fd at 23 °C shows broadened signals, which are clearly shifted outside the diamagnetic envelope, indicating that they correspond to the protons located in the proximity of the paramagnetic centers (Figure 4). These resonances have been assigned to the β-CH_2 protons of the seven cysteine residues involved in the coordination of the two cubic FeS clusters of *Aa*Fd, at pH 7 (*11*) (Scheme 1). The intensities and positions of the NMR signals are unaltered at pH 2.5 (not shown), corroborating that the protein and its metal centers remain structurally intact in acidic conditions. The thermal perturbation was followed by the decrease of intensity and areas of the assigned resonances as a function of the incubation temperature (Figure 5, Table 1). The differences in the T_m^{app} of the individual cysteine ligands are very small. Only Cys^{89} from the [4Fe4S] has a slightly higher T_m^{app} than the average of the other ligands (∼5 °C). The enhanced stability of the Cys^{89} ligand may originate from stabilizing apolar interactions in its vicinity. Inspection of *Aa*Fd structure suggests that the adjacent Val^{90} and nearby Ile^{98} and Val^{100} may be involved in such stabilization.

CONCLUSIONS

The body of spectroscopic data accumulated in the present work provides a framework for understanding of the structural and dynamical modifications of *Aa*Fd during thermal perturbation. Changes in metalloprotein organization are clearly intertwined with disassembly of the iron−sulfur centers, denoting the conformational interplay of the cofactors and the protein backbone (Scheme 2). Thermally induced unfolding of *Aa*Fd is initiated with the loss of α-helical content at relatively low temperatures (T_m^{app} ∼ 44 °C), followed by the disruption of both iron−sulfur clusters (T_m^{app} ∼ 53−60 °C). The observed disruption of α-helices

Scheme 2: Structural Model of *Aa*Fd in Two Orthogonal Views

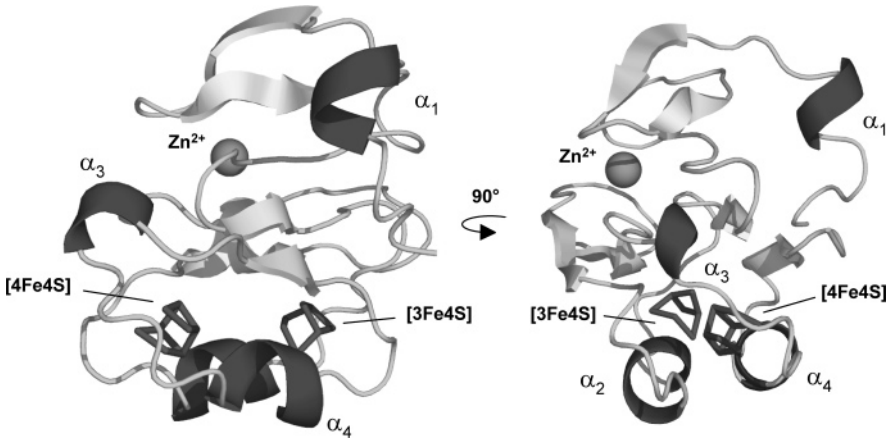

occurring at ~44 °C may be hypothesized to involve mostly helices α1 and α3, which are located far from the protein $(\beta\alpha\beta)_2$ core in which the helices α2 and α4, that provide coordinating cysteines for the iron−sulfur clusters, are found. It is feasible to speculate that the latter helices undergo a conformational distortion concomitantly with the clusters' disruption, at higher temperatures (Scheme 2). RR and NMR data indicate that the last steps in the disassembly of the clusters are the disruption of the terminal Cys^{89} ligand from the [4Fe4S] center and of the bridging ligands of the [3Fe4S] cluster. The degradation of the metal centers triggers major structural changes of the protein matrix, including the loss of tertiary contacts ($T_m^{app} \sim 58$ °C) and a change, rather than a significant net loss, of secondary structure ($T_m^{app} \sim 60$ °C). Thus, the final product of thermal perturbation of *Aa*Fd is an apo *Aa*Fd which has features of a molten globule. The combined spectroscopic approach employed here has proven capable of providing a detailed description of the unfolding mechanism of iron−sulfur proteins, paving the way for future studies.

ACKNOWLEDGMENT

C. Frazão (ITQB, Oeiras) is gratefully acknowledged for *A. ambivalens* Fd coordinates, M. Teixeira (ITQB, Oeiras) for a cytosolic fraction of *A. ambivalens*, and B. O. Kolbesen (Johann Wolfgang Goethe-Universität, Frankfurt) for TXRF metal analysis.

REFERENCES

1. Wittung-Stafshede, P., Gomes, C. M., and Teixeira, M. (2000) Stability and folding of the ferredoxin from the hyperthermophilic archaeon Acidianus ambivalens, *J. Inorg. Biochem. 78*, 35−41.
2. Leal, S. S., Teixeira, M., and Gomes, C. M. (2004) Studies on the degradation pathway of iron-sulfur centers during unfolding of a hyperstable ferredoxin: cluster dissociation, iron release and protein stability, *J. Biol. Inorg. Chem. 9*, 987−996.
3. Leal, S. S., and Gomes, C. M. (2005) Linear three-iron centres are unlikely cluster degradation intermediates during unfolding of iron-sulfur proteins, *Biol. Chem. 386*, 1295−1300.
4. Fujii, T., Hata, Y., Oozeki, M., Moriyama, H., Wakagi, T., Tanaka, N., and Oshima, T. (1997) The crystal structure of zinc-containing ferredoxin from the thermoacidophilic archaeon Sulfolobus sp. strain 7, *Biochemistry 36*, 1505−1513.
5. Gomes, C., Faria, A., Carita, J., Mendes, J., Regalla, M., Chicau, P., Huber, H., Stetter, K., and Teixeira, M. (1998) Di-cluster, seven-iron ferredoxins from hyperthermophilic Sulfolobales, *J. Biol. Inorg. Chem. 3*, 499−507.
6. Kojoh, K., Matsuzawa, H., and Wakagi, T. (1999) Zinc and an N-terminal extra stretch of the ferredoxin from a thermoacidophilic archaeon stabilize the molecule at high temperature, *Eur. J. Biochem. 264*, 85−91.
7. Rocha, R., Leal, S. S., Teixeira, V. H., Regalla, M., Huber, H., Baptista, A. M., Soares, C. M., and Gomes, C. M. (2006) Natural domain design: enhanced thermal stability of a zinc-lacking ferredoxin isoform shows that a hydrophobic core efficiently replaces the structural metal site, *Biochemistry 45*, 10376−10384.
8. Leal, S., and Gomes, C. M. (2007) Studies of the molten globule state of ferredoxin: structural characterisation and implications on protein folding and iron-sulfur centre assembly, *Proteins 68*(3), 606−616.
9. Teixeira, M., Batista, R., Campos, A. P., Gomes, C., Mendes, J., Pacheco, I., Anemuller, S., and Hagen, W. R. (1995) A seven-iron ferredoxin from the thermoacidophilic archaeon Desulfurolobus ambivalens, *Eur. J. Biochem. 227*, 322−327.
10. Semisotnov, G. V., Rodionova, N. A., Razgulyaev, O. I., Uversky, V. N., Gripas, A. F., and Gilmanshin, R. I. (1991) Study of the "molten globule" intermediate state in protein folding by a hydrophobic fluorescent probe, *Biopolymers 31*, 119−128.
11. Bentrop, D., Bertini, I., Luchinat, C., Mendes, J., Piccioli, M., and Teixeira, M. (1996) Paramagnetic NMR analysis of the seven-iron ferredoxin from the hyperthermoacidophilic archaeon Desulfurolobus ambivalens reveals structural similarity to other dicluster ferredoxins, *Eur. J. Biochem. 236*, 92−99.
12. Czernuszewicz, R. S., Macor, K. A., Johnson, M. K., Gewirth, A., and Spiro, T. G. (1987) Vibrational-Mode Structure and Symmetry in Proteins and Analogs Containing Fe4S4 Clusters - Resonance Raman Evidence for Different Degrees of Distortion in Hipip and Ferredoxin, *J. Am. Chem. Soc. 109*, 7178−7187.
13. Duin, E. C., Lafferty, M. E., Crouse, B. R., Allen, R. M., Sanyal, I., Flint, D. H., and Johnson, M. K. (1997) [2Fe-2S] to [4Fe-4S] cluster conversion in Escherichia coli biotin synthase, *Biochemistry 36*, 11811−11820.
14. Han, S., Czernuszewicz, R. S., Kimura, T., Adams, M. W. W., and Spiro, T. G. (1989) Fe2S2 Protein Resonance Raman-Spectra Revisited - Structural Variations among Adrenodoxin, Ferredoxin, and Red Paramagnetic Protein, *J. Am. Chem. Soc. 111*, 3505−3511.
15. Iwasaki, T., Watanabe, E., Ohmori, D., Imai, T., Urushiyama, A., Akiyama, M., Hayashi-Iwasaki, Y., Cosper, N. J., and Scott, R. A. (2000) Spectroscopic investigation of selective cluster conversion of archaeal zinc-containing ferredoxin from Sulfolobus sp strain 7, *J. Biol. Chem. 275*, 25391−25401.
16. Johnson, M. K., Czernuszewicz, R. S., Spiro, T. G., Fee, J. A., and Sweeney, W. V. (1983) Resonance Raman-Spectroscopic Evidence for a Common [3Fe-4S] Structure among Proteins Containing 3-Iron Centers, *J. Am. Chem. Soc. 105*, 6671−6678.
17. Glasoe, P. K., and Long, F. A. (1960) Use of Glass Electrodes to Measure Acidities in Deuterium Oxide, *J. Phys. Chem. 64*, 188−190.
18. Arrondo, J. L., Muga, A., Castresana, J., and Goni, F. M. (1993) Quantitative studies of the structure of proteins in solution by Fourier-transform infrared spectroscopy, *Prog. Biophys. Mol. Biol. 59*, 23−56.
19. Byler, D. M., and Susi, H. (1986) Examination of the secondary structure of proteins by deconvolved FTIR spectra, *Biopolymers 25*, 469−487.
20. Dong, A., Kendrick, B., Kreilgard, L., Matsuura, J., Manning, M. C., and Carpenter, J. F. (1997) Spectroscopic study of secondary structure and thermal denaturation of recombinant human factor XIII in aqueous solution, *Arch. Biochem. Biophys. 347*, 213−220.
21. Jackson, M., and Mantsch, H. H. (1995) The use and misuse of FTIR spectroscopy in the determination of protein structure, *Crit. Rev. Biochem. Mol. Biol. 30*, 95−120.
22. Kunihiro, K., and Arai, M. (2000) The molten globule state: the physical picture and biological significance, in *Mechanisms of Protein Folding* (Pain, R. H., Ed.) Oxford University Press: Oxford.
23. Stephens, P. J., Jensen, G. M., Devlin, F. J., Morgan, T. V., Stout, C. D., Martin, A. E., and Burgess, B. K. (1991) Circular dichroism and magnetic circular dichroism of Azotobacter vinelandii ferredoxin I, *Biochemistry 30*, 3200−3209.
24. Stephens, P. J., Thomson, A. J., Dunn, J. B., Keiderling, T. A., Rawlings, J., Rao, K. K., and Hall, D. O. (1978) Circular dichroism and magnetic circular dichroism of iron-sulfur proteins, *Biochemistry 17*, 4770−4778.
25. Lutz, M., Moulis, J. M., and Meyer, J. (1983) Resonance Raman-Spectroscopy of Azotobacter-Vinelandii Ferredoxin. 1. Vibrational Features of the [3Fe-3S] Cluster, *FEBS Lett. 163*, 212−216.

BI700967G